Selenographic Coordinate Mapping of Lunar Observation by GOES Imager

Xi Shao[1,2], Xiangqian Wu[3], Fangfang Yu[1]

[1]Earth Resource Technology, Inc., Laurel, MD, USA
[2] University of Maryland, College Park, MD, USA
[3]NOAA/NESDIS/STAR, College Park, MD, USA

ABSTRACT

Radiometric stability of the lunar surface, its lack of atmosphere and smooth reflectance spectrum makes the moon an ideal target for calibrating satellite-based multi-band imagers. Lunar calibration for solar bands has been an important part of trending the radiometric performance of GOES imager. The lunar disk-equivalent irradiance has been often used to trend the on-orbit degradation of the GOES imager and its performance is largely affected by the uncertainties embedded in the lunar irradiance model in characterizing its dependence on lunar phase and libration. On the other hand, the lunar view by GOES imager provides opportunity to perform radiometric calibration of GOES imager using lunar radiances of selected locations on the moon. In order to do so, lunar observations by GOES need to be mapped onto selenographic coordinate, i.e. latitude and longitude in moon-centered coordinate. In this paper, algorithms and procedures are developed to map lunar images observed by GOES onto selenographic coordinate. Progressive shift in east-west scan direction, oversampling factor and distortion of lunar image are corrected to transform it back to be within a circular disk. Controlling region matching is applied to determine rotation angle and three consecutive rotations are performed to map lunar observation onto selenographic coordinate. Lunar observations of GOES-12 are processed and regions of interest (ROIs) are identified. Lunar phase-dependence of lunar measurements at ROIs is analyzed. It is found that lunar measurement depends strongly on Sun-Moon-Satellite geometry and knowledge of BRDF of lunar surface can enable trending of radiometric performance of GOES imager with local lunar radiance.

Keywords: lunar calibration, lunar radiance calibration, GOES lunar observation, selenographic coordinate mapping

1. INTRODUCTION

The Geostationary Operational Environmental Satellite (GOES) is a series of geostationary satellites that have been making continuous measurements of the surface and atmosphere of the Western Hemisphere since the late 1970s, providing valuable information for weather forecast and climate change studies. The visible channel of the GOES Imager degrades over time and does not have an onboard calibration device. Quantitative analyses for weather forecast and long-term monitoring of climate change using GOES imagery require accurate calibration of the instrument and assessment of sensor system response changes over time. Several methods have been developed for vicarious calibration of the GOES Imager visible channel. These include methods based on the sensor's measurements of celestial bodies such as the Moon [1-3] and stars [4-5], stable Earth targets such as desert [6-13], deep convective clouds (DCCs) [14], and well-calibrated instruments onboard low Earth orbit (LEO) satellites [15-17]. Operationally, the degradation of visible channel of GOES Imager has been determined using an integrated calibration approach which combines vicarious calibration methods such as deep convective cloud, stable desert site and ray-matching methods [13].

Radiometric stability of the lunar surface and its smooth reflectance spectrum makes the moon an ideal target for calibrating satellite-based visible imagers [18-24]. GOES Imager has a rectangular field of regard including margins and corners that view deep space. The Moon appears regularly in these areas. Lunar calibration for visible channel has been an important part of trending and validating the radiometric performance of GOES Imager. The lunar disk-equivalent irradiance has been used to trend the on-orbit degradation of the GOES imager [3]. The lunar irradiance depends on the Sun-Moon-Earth geometry and it is a strong function of lunar phase. In addition, the lunar irradiance is also affected by lunar libration since a little more than half (59%) of Moon surface can be seen from Earth over different times. Therefore, the performance of calibrating satellite radiometer using Moon is largely affected by the uncertainties

Sensors, Systems, and Next-Generation Satellites XIX, edited by Roland Meynart, Steven P. Neeck, Haruhisa Shimoda, Toshiyoshi Kimura, Proc. of SPIE Vol. 9639, 963918 · © 2015 SPIE
CCC code: 0277-786X/15/$18 · doi: 10.1117/12.2193914

embedded in the lunar irradiance model such as USGS RObotic Lunar Observatory (ROLO) model [20] in characterizing its dependence on lunar phase and libration. While Moon is capable of providing high relative calibration accuracy for the solar reflective channels, no reliable absolute lunar irradiance model is currently available for the purpose of absolute calibration.

On the other hand, the lunar view by GOES Imager is of high spatial resolution and provides opportunity to perform radiometric calibration of GOES imager using lunar radiances collected from selected locations on the moon. The radiance of the Moon spans roughly half the dynamic range of a typical Earth scene, but covers all of the range of clear ocean and most of that of clear land. The lunar view by GOES Imager is oversampled in East/West direction, skewed due to the orbital motion of the moon, rotated and projected into the plane perpendicular to the direction of Moon-satellite. In order to register the lunar radiance from GOES observation onto the same location on lunar surface, lunar observations by GOES need to be mapped onto selenographic coordinate, i.e. latitude and longitude in moon-centered coordinate.

In this paper, methods based on image processing and coordinate transformation are developed to map lunar images observed by GOES onto selenographic coordinate. The selenographic coordinate-mapping methods first correct progressive shift in east-west scan direction, oversampling factor and distortion of lunar image and transform it back to be within a disk. Next, controlling region matching methods applied to determine relative rotation angles and three consecutive rotations are performed to map lunar observation onto selenographic coordinates. Section 2 describes the lunar observations by GOES-12 Imager visible channel that are being processed in this paper. Section 3 describes the algorithm and processing steps that have been developed to map lunar images observed by GOES onto selenographic coordinate. Section 4 investigates the characteristic dependence of lunar measurement over regions of interest (ROIs) vs. lunar phase angle. Uncertainties embedded in the mapping method are also discussed.

2. DATA COLLECTION

The lunar observations analyzed in this study were performed by visible channel of GOES-12 Imager. GOES-12 visible channel covers wavelength range from 0.5 um to 0.8 um. There have been two types of lunar observations by GOES-12 Imager: observation by opportunity, i.e. lunar appearance during the full disk scan, and scheduled lunar view.

During normal GOES operations, GOES Imager takes full-earth imagery every three hours within a rectangular field of regard (FOR) of 21° N-S by 19.2° E-W. The Earth disk diameter is about 17.4◦ from geostationary orbit. The FOR of GOES Imager full disk scan has margins around the Earth disk (~1.8◦ in N-S and ~0.9◦ in E-W, respectively), scanning past the limb and viewing deep space. The Moon appears regularly in the area between the limb of Earth disk and the rectangular FOR. From geostationary orbit, the Moon's diameter varies between 0.44◦ and 0.51◦. GOES visible imager detector has instantaneous field of view of 28 μrad in N-S and effective E–W sample size of 16 μrad. Therefore, full moon at perigee covers ~ 318 N–S lines by ~556 E–W pixels in GOES Imager. Figure 1 shows an example, in which the moon is in the upper left corner of the GOES-12 full Disk image around 17:45 UTC on September 19, 2005. The moon appears tilted due to the motion of the satellite during the image acquisition time.

Lunar appearance by opportunity during the full disk scan can't guarantee routine lunar observations to support lunar calibration since GOES is operated on a complicated schedule and it images various sectors within its FOR at different frequency and Moon-view opportunities with suitable lunar phases can often be missed. Since November 2005, NOAA started scheduled lunar image collection and made use of field of view (FOV) (21° N-S by 23° E-W) of GOES Imager. Predictions of suitable Moon appearances are routinely performed and satellite operations are informed in advance to replace scheduled star views with lunar view. This practice demonstrated that scheduled collection of GOES lunar images is feasible and sustainable in GOES operation. It is done about once or twice a month for each satellite, and lasts about one minute each time.

In total, there are 52 lunar observations identified from GOES-12 Imager data from year 2003 to 2010 with lunar phases varying between -80 and 80 degree. In order to have adequate visible lunar surface area so that the moon has abundant features for selenographic coordinate mapping, we select cases for in this study having absolute value of lunar phase less than 50 degree. In total, 44 lunar observations by GOES-12 Imager are selected. Figure 2 shows the distribution of lunar phase for the 44 events selected.

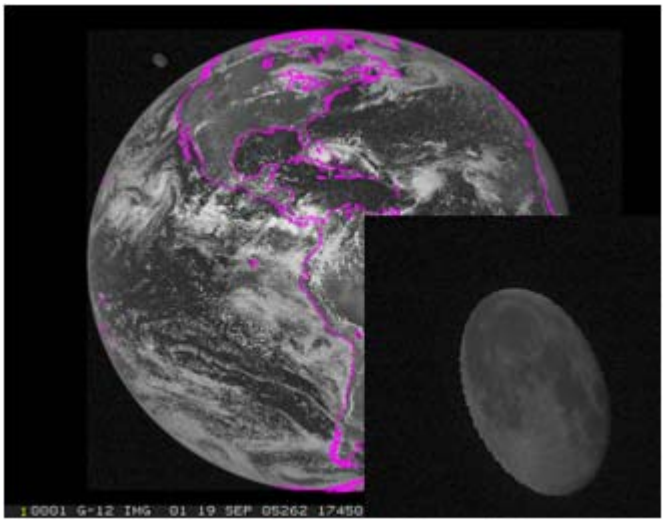

Figure 1: Example of GOES-12 lunar view relative to full disk image of Earth around 17:45 UTC on Sept. 19, 2005. The moon appears in the upper left corner, and is shown enlarged in the insert.

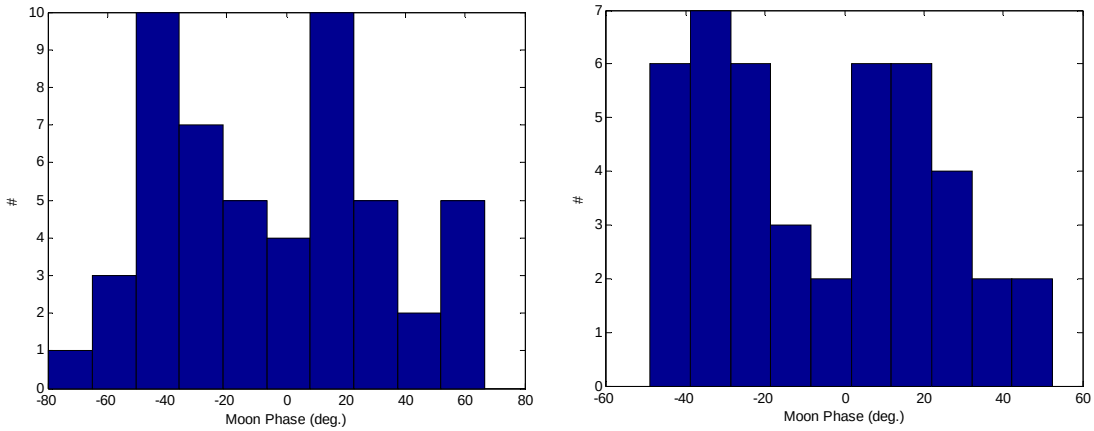

Figure 2: Distribution of lunar phase from lunar observations of GOES-12 (left) and the distribution of selected 44 events with |lunar phase| < 50 degree (right).

3. METHODOLOGY

The lunar images observed by GOES Imager are in two-dimension and have been projected onto a plane perpendicular to the Moon-satellite vector. Using the celestial object tracking software and given the satellite position, the Moon-satellite vector can be accurately calculated in selenographic coordinate, i.e. (θ_s, α_s), where θ_s and α_s is the longitude and latitude of the satellite, respectively. To map lunar image from GOES onto selenographic coordinate, we need to first correct progressive shift in east-west scan direction and oversampling factor, and transform the image to be within a circular disk. Due to variation in the view orientation of GOES Imager, for a given pixel on the transformed lunar disk with coordinate (r, φ) in polar coordinate, it is rotated around its center by an angle of $\delta\varphi = \varphi_s - \varphi$ relative to the actual coordinate (r, φ_s) projected from the selenographic coordinate. Therefore, method of controlling region matching is used to determine the relative rotation angle $\delta\varphi$. In this method, a template region has been identified with known coordinate and cross-correlation between the template pixels and lunar image to be mapped are calculated to determine the angle $\delta\varphi$. Having determined the angles (θ_s, α_s, $\delta\varphi$), three consecutive rotations are performed to map lunar observation onto selenographic coordinates. Finally, a landmark such as Tycho crater with apparent texture and known coordinate used in this study, is used to validate and fine tune the coordinate transformation. Details of processing steps are illustrated as following.

Step 1: Correcting lunar image to be within a circular disk

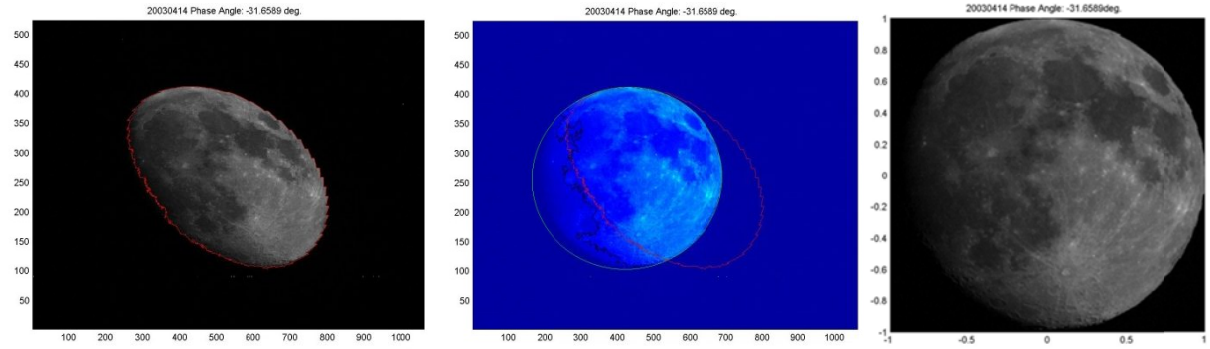

(a) (b) (c)

Figure 3: (a) Lunar image observed by GOES-12 on 2003/04/14 with boundary marked with red contour line which is identified through boundary detection; (b) The processed lunar image after applying correction for skewed saw-tooth boundary on East side. Red contour line marks the location of the original lunar boundary. Black line marks the contour bounary of porcessed lunar image with skewed saw-tooth boundary correction. Light blue line marks the fitted ellipse. Note that E-W (horizontal) and N-S (vertical) axies are of different scale. (c) The transformed lunar image within a circular disk in normalized coordinate.

Figure 3a shows an example of typical lunar image observed by GOES-12 Imager around 14:48 on 2003/04/14. The lunar phase for this event is -31.66 degree with the negative sign meaning a waxing moon. The moon in GOES images appears skewed due to the satellite orbital motion during the image acquisition time which renders an eastward movement of ~15.04º/hr or ~0.25º/min for the moon. In addition, saw-tooth pattern of scan line offsets can be seen at the East and West limbs of the lunar image. This is due to the progressive shift of scan line blocks toward the East side. The scan lines within the same block have the same offset and this offset varies from block to block, thus forming the saw-tooth boundary. From Figure 3a, it can be identified that the round edge of the moon is on the East wide of the image. To correct the saw-tooth boundary due to eastward shift of the scan line blocks, the lunar boundary is first determined with boundary detection (see red line in Figure 3a). On the East side of the lunar boundary, the difference δX_i between the X positions of boundary pixels on adjacent (i and i+1) scan lines are calculated. A threshold δX_t is determined so that $\delta X_i > \delta X_t$ indicates the discontinuity in the boundary of lunar image and the formation of scan line blocks. The scan lines in-between boundary discontinuity can be grouped to be within the same block with the same offset. Then, the skewed saw-tooth lunar boundary is corrected by shifting scan line blocks westward with corresponding offsets. The resulting lunar image after the correction is shown in Figure 3b. Note that E-W (horizontal) and N-S (vertical) axies of Figure 3b are of different scale and the correted lunar image is a slightly titled ellipse. Further processing needs to be perfromed to correct it to be within a circular disk.

For moon with |lunar phase angle| larger than 0 degree, i.e. non-full moon, the lunar disk is partially dark on one side and has round edge on the other side. For example, the lunar image in Figure 3b has round edge on the East side and is partially dark on the West side, which can been identified with the black contour line in the figure. To perform elliptic fitting for the lunar image, segment of the smooth boundary need to be used for fitting. Therefore, smoothness of the lunar boundary, *i.e.* black line in Figure 3b, is calculated and segment of the smooth boundary is identified. Then, elliptic fitting is applied to determine the elliptic parameters such as center, tilt angle, major and minor axis of the ellipse. Blue line in Figure 3b shows the fitted ellipse. The difference between lengths of major and minor elliptic axies is due to oversampling and the ratio between them has been determined to be ~1.75. With the elliptic parameters obtained from fitting, the lunar image can be transformed to be within a circular disk after correcting the oversampling factor. Figure 3c shows the thus determined circular lunar disk in normalized coordinate.

Step 2: Controlling region matching

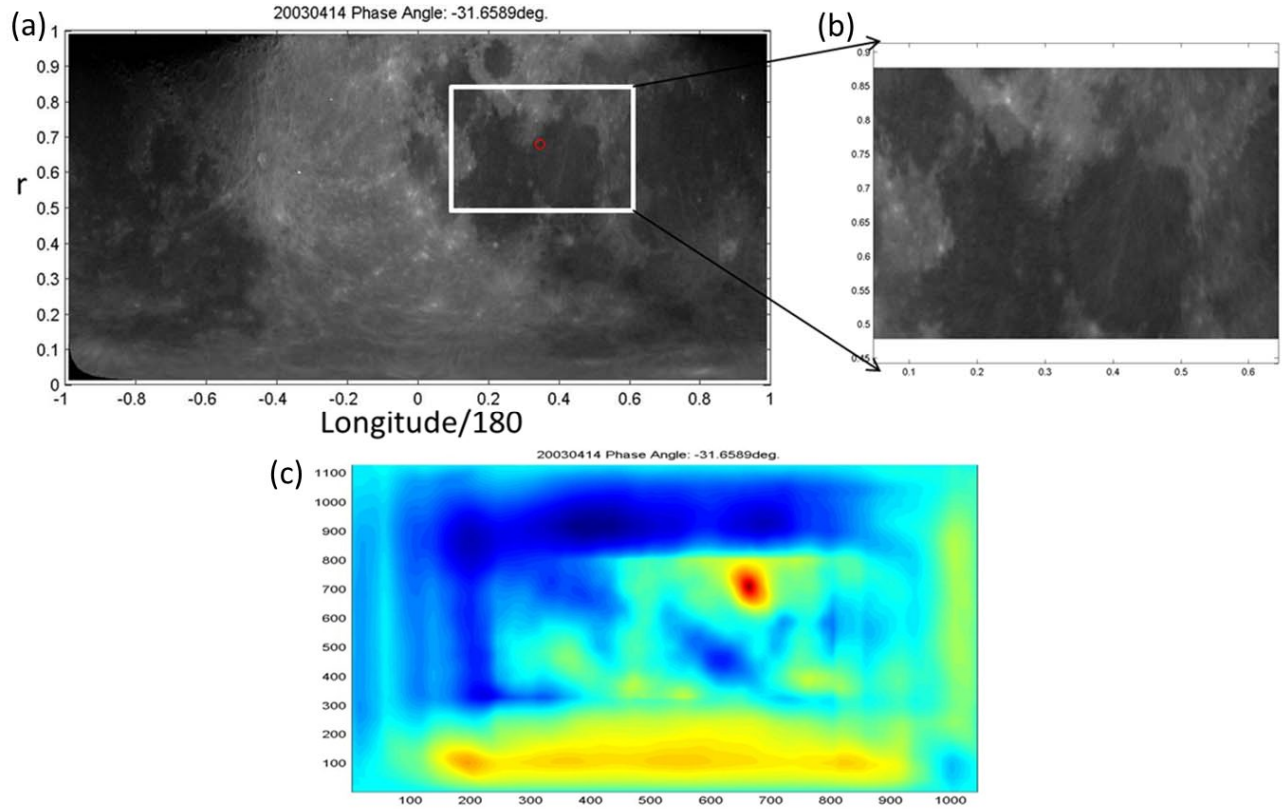

Figure 4: (a) Example of unfolded lunar image in Longitude/180-r coordinate for lunar observation on 2003/04/14 by GOES-12; (b) A template is extracted from lunar image with high contrast bright and dark features and of known selenographic coordinate. This template is later used for calculating cross-correlation map with other lunar observations to determine the rotation angle $\delta\varphi$ for those events. (c) Cross-correlation map calculated between the template in (b) and image in (a).

Due to variation in the view orientation of GOES Imager, the transformed lunar image such as that in Figure 3c has been rotated around its center by an angle $\delta\varphi = \varphi_s - \varphi$ relative to the actual longitude φ_s projected from the selenographic coordinate, where φ is the longitude for a given pixel on the transformed lunar disk in polar coordinate. To determine the relative rotation angle $\delta\varphi$, method of controlling region matching is used. First, the lunar disk image such as that in Figure 3c is unfolded onto Cartesian coordinate, i.e. normalized longitude (longitude/180) vs. r coordinate, and interpolated onto uniform grid. See Figure 4a for an example. A template region with known coordinate, high contrast lunar features and containing both highland and mare is selected. An example of such template used in this study is shown in Figure 4b. This template center has a known longitude φ_{st} as projected from the selenographic coordinate. Cross-correlation between the pixels in the template and the lunar image to be mapped is calculated and a cross-correlation matrix is constructed. Figure 4c shows such a cross-correlation map constructed between the template in Figure 4b and the unfolded lunar image in Figure 4a. In this case, since the template is a section extracted from the original map in Figure 4a, the correlation coefficient reaches maximum = 1 (dark red dot in Figure 4c) at where the center of the template is located. For lunar observations by GOES Imager at other times different from the time of the template, the maximum cross-correlation coefficient is usually less than 1 due to different view geometry, different lunar phase, and uncertainties in the observation and mapping. Given the longitude of the central pixel with maximum correlation, i.e. φ_m, on the unfolded image, the rotation angle $\delta\varphi$ can be thus determined as $\delta\varphi = \varphi_{st} - \varphi_m$ with controlling region matching.

Step 3: Coordinate Transformation

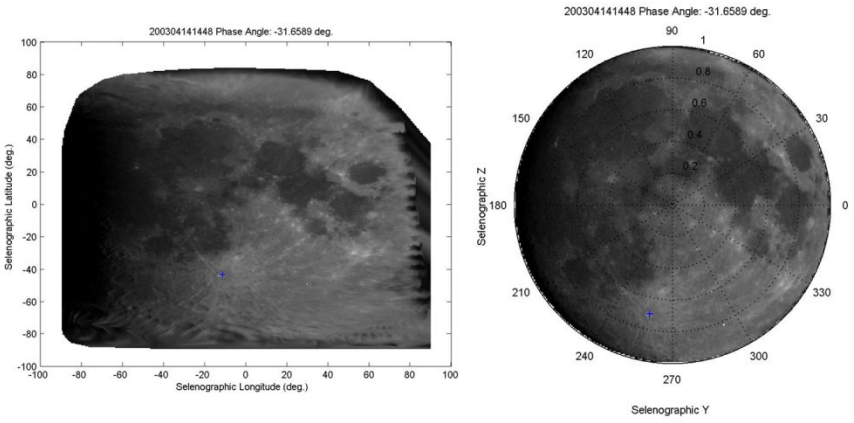

Figure 5: (a) Mapped lunar image for GOES-12 observation around 14:48 on 2004/04/14 in selenographic longitude vs. latitude coordinate; (b) lunar image mapped onto selenographic Y-Z coordinate. Blue '+' marks location of Tycho crater.

The lunar image observed by GOES Imager is an image projected onto a plane perpendicular to the Moon-satellite vector. The Moon-satellite vector can be accurately determined in selenographic coordinate and expressed as (θ_s, α_s), where θ_s and α_s is the longitude and latitude of the satellite, respectively. From Step 1 and 2, we have determined the angles (θ_s, α_s, $\delta\varphi$). For a given pixel (r, φ) on projected lunar disk, three consecutive rotations (Eq. 1) are performed to map pixels in lunar image onto Cartesian selenographic coordinate.

$$\begin{bmatrix} X \\ Y \\ Z \end{bmatrix} = \begin{bmatrix} \cos(\theta_s) & -\sin(\theta_s) & 0 \\ \sin(\theta_s) & \cos(\theta_s) & 0 \\ 0 & 0 & 1 \end{bmatrix} \begin{bmatrix} \cos(\alpha_s) & 0 & \sin(\alpha_s) \\ 0 & 1 & 0 \\ -\sin(\alpha_s) & 0 & \cos(\alpha_s) \end{bmatrix} \begin{bmatrix} 0 \\ r\cos(\varphi + \delta\varphi) \\ r\sin(\varphi + \delta\varphi) \end{bmatrix} \quad (1)$$

After obtaining Cartesian coordinate (X, Y, Z) for a pixel, selenographic longitude and latitude can be determined through Cartesian-spherical coordinate transformation.

Step 4: Validation Site

Having mapped the lunar image by GOES Imager onto selenographic coordinate, a landmark site on Moon surface with apparent texture features is used to validate and fine tune the coordinate transformation. In this study, Tycho crater (latitude: 43.31°S; longitude: 11.36°W) on lunar surface is used as such a validation site. The location of Tycho crater is marked as the blue '+' in Figure 5a and 5b.

4. EXAMPLE OF MAPPING LUNAR IMAGE

Figures 6-8 show examples of applying the algorithm and processing steps we developed to map GOES-12 lunar observations onto selenographic coordinate for several typical scenarios. Figure 6 shows steps of mapping lunar observation observed on 2004/05/03 15:10 onto selenographic coordinate. For this observation, the lunar phase is -18.24 degree and it is a waxing moon. Figure 6d shows the cross-correlation map between the template in Figure 4b (extracted from observation on 2003/04/14) and lunar image in Figure 6c (observed on 2004/05/03). The maximum correlation can be clearly identified as the dark red dot on the map and the rotation angle $\delta\varphi$ is therefore determined. The mapped lunar image in selenographic coordinate is shown in Figure 6e with Tycho crater marked as blue '+'.

Figure 7 shows another example of mapping GOES-12 lunar observations on 2005/10/14 onto selenographic coordinate. The lunar phase is -37.16 degree for this case and the bottom part of the lunar image in Figure 7a is shited eastward with an apparent discontinuity. The algorithm described in Section 3 is robust enough to correct the lunar image to be within a circular disk. The location of the template we used (Figure 4b) is clearly identified with controlling region matching (Figure 7b), and the lunar image is correctly transformed onto selenographic coordinate (Figure 7c) after validation with the Tycho crater site (marked as blue '+'). Both cases in Figure 6 and 7 are waxing moon and the dark side the moon appears on the West side after the mapping.

Figure 8 shows a third example of mapping GOES-12 lunar observations on 2006/02/14 onto selenographic coordinate. In this case, the lunar phase is 16.23 degree and of waning phase. The moon is partially dark on East side and has round edge on the West side. Therefore, the saw-tooth boundary to be processed in Step 1 is on the West side of the lunar image. In doing so, the lunar image is first flipped in East-West direction and Step 1 processing is applied to the image. After scaling the lunar image to be within a circular disk, the image is flipped back horizontally and processing Step 2-4 are apllied afterwards. Figure 8b and 8c shows that the processing algorithm we developed is also effective in mapping Moon with waning phase onto selenographic coordinate.

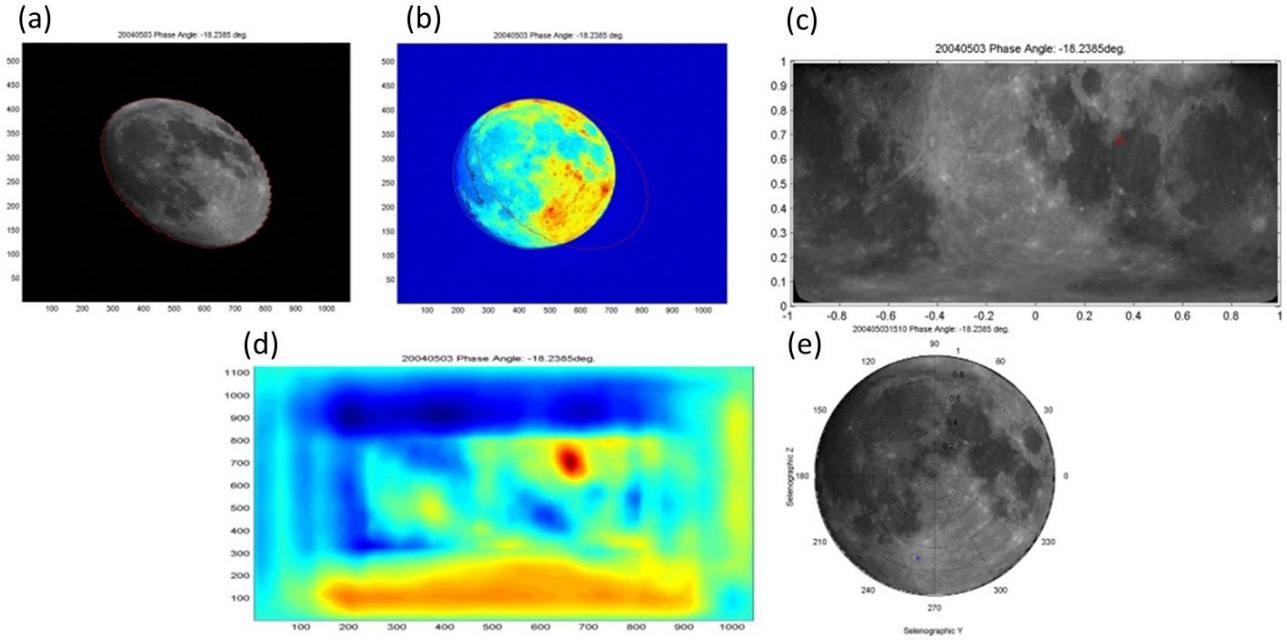

Figure 6: (a) Lunar image observed by GOES-12 around 15:10 on 2004/05/03 with boundary marked with red contour line; (b) The processed lunar image after applying skewed saw-tooth boundary correction. Red and black line mark the boundary of original and porcessed lunar image with correction, respectively. Light blue line marks the fitted ellipse. (c) unfolded lunar image in Longitude/180-r coordinate; (d) Cross-correlation map calculated between the template in Figure 4b (extracted from observation on 2003/04/14) and lunar image in (c). (e) Lunar image mapped onto selenographic Y-Z coordinate. Blue '+' marks location of Tycho crater.

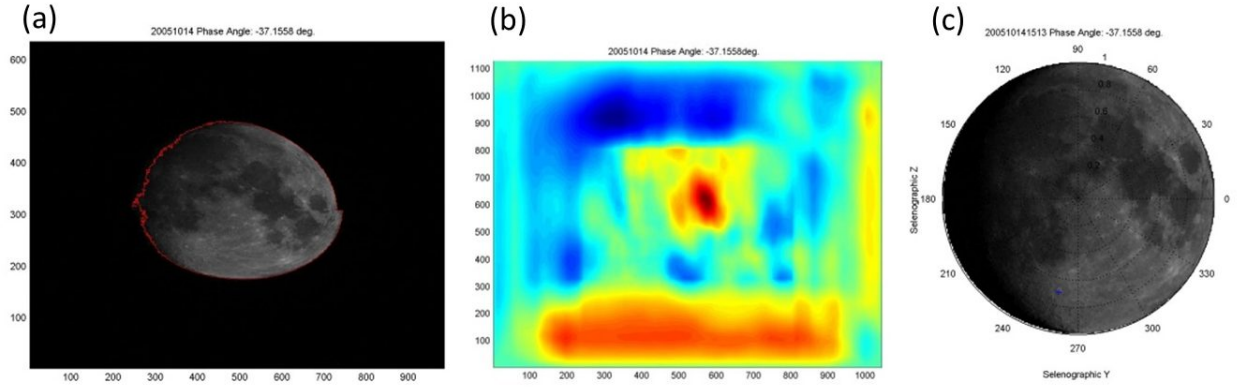

Figure 7: An example of applying the algroithm to process lunar observation on 2005/10/14 15:13 (panel (a)) onto selenographic coordinate (panel (c)) through controlling region matching by using cross-correlation map (panel (b)).

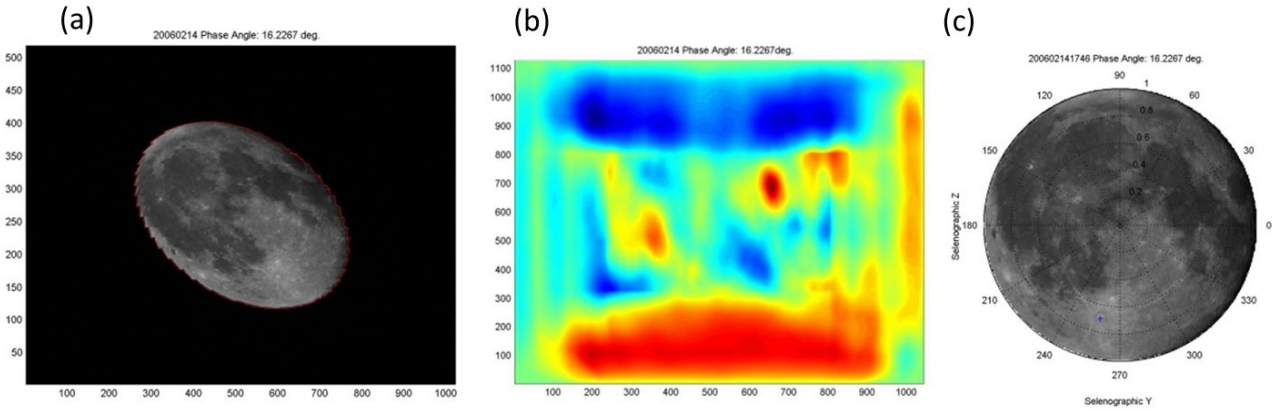

Figure 8: An example of applying the algroithm to process lunar observation on 2006/02/14 17:46 (panel 8a) onto selenographic coordinate (panel 8c) through controlling region matching by using cross-correlation map (panel 8b). Note that the saw-tooth boundary to be processed is on the West side of the lunar image due to waning moon.

5. DEPENDENCE OF LUNAR MEASUREMENT AT ROIS ON LUNAR PHASE

Those 44 lunar observations by GOES-12 with |lunar phase| < 50 degree have been processed and mapped onto selenographic coordinate by applying the processing algorithm we developed. The lunar measurement by GOES-12 is in digital count (DC). After subtracting the background offset (DC_0), the lunar data needs to be corrected with trending function to account for degradation of GOES Imager. In [13], the degradation of visible channel of GOES-12 Imager has been determined as a function of time $f(t)$ by employing an integrated calibration method which combines three vicarious calibration methods such as deep convective cloud, stable desert site and ray-matching methods. This trending function has been applied to the offset-corrected DC of lunar measurement and the derived lunar data is called trend-corrected DC. The trend-corrected DC can be converted to lunar radiance by multiplying a constant factor.

Six regions of interest (ROIs) (see Figure 9a and 9b) have been chosen to study the dependence of lunar measurements at these ROIs on lunar phase. Among these ROIs, ROI #1 is at the center of selenographic coordinate and ROI #2 is at Tycho crater. ROI #2 and #3 have more highland and are bright. ROI #4-6 have more mare and are relatively dark. A rectangular region of size $\delta Y = 0.1$ by $\delta Z = 0.1$ around the ROI on the projected selenographic Y-Z coordinate has been chosen and trend-corrected lunar DC data for pixels within the region are collected. Mean value of these pixels is derived as the characteristic lunar measurement for the ROI. As shown in Figure 2, the 44 selected GOES 12 lunar observations have an evenly distributed lunar phases ranging from -50 degree to 50 degree. Here, the lunar phase is the angle formed between Sun-Moon and Moon-Satellite vectors with waxing being negative phase and waning being positive phase, respectively. The characteristic trend-corrected lunar DC data for 6 ROIs derived from these 44 observations are plotted against lunar phase in Figure 10. For all of these 6 ROIs, the trend-corrected DC is well organized by lunar phase, which peaks at lunar phase = 0 degree and decreases as the |lunar phase| increases. There is a sharp rise in DC when phase angle approaches zero (close to full moon), which is due to opposition effect with ROI being illuminated from directly behind the satellite. The dependence of trend-corrected lunar DC on lunar phase for 6 ROIs is in general asymmetric between negative and positive, i.e. waxing and waning, lunar phases. The asymmetry is the strongest for ROI #4-6, which has lower DC value due to having features of dark mare. This suggests that accurate knowledge of BRDF of lunar surface is important to trend radiometric performance of GOES Imager with lunar radiance and further study will be performed.

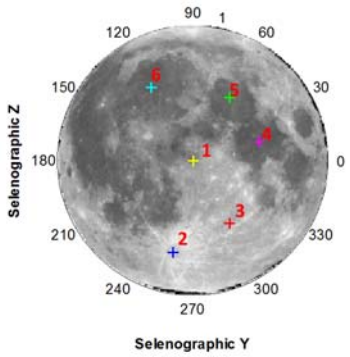

	Latitude	Longitude
1	0	0
2	-43.31	-11.36
3	-28	18
4	8	30
5	28	18
6	33	-21.5

Figure 9: (Left) Location of selected ROIs on lunar surface. (Right) Selenographic latitude and longtitude (in degree) of selected ROIs.

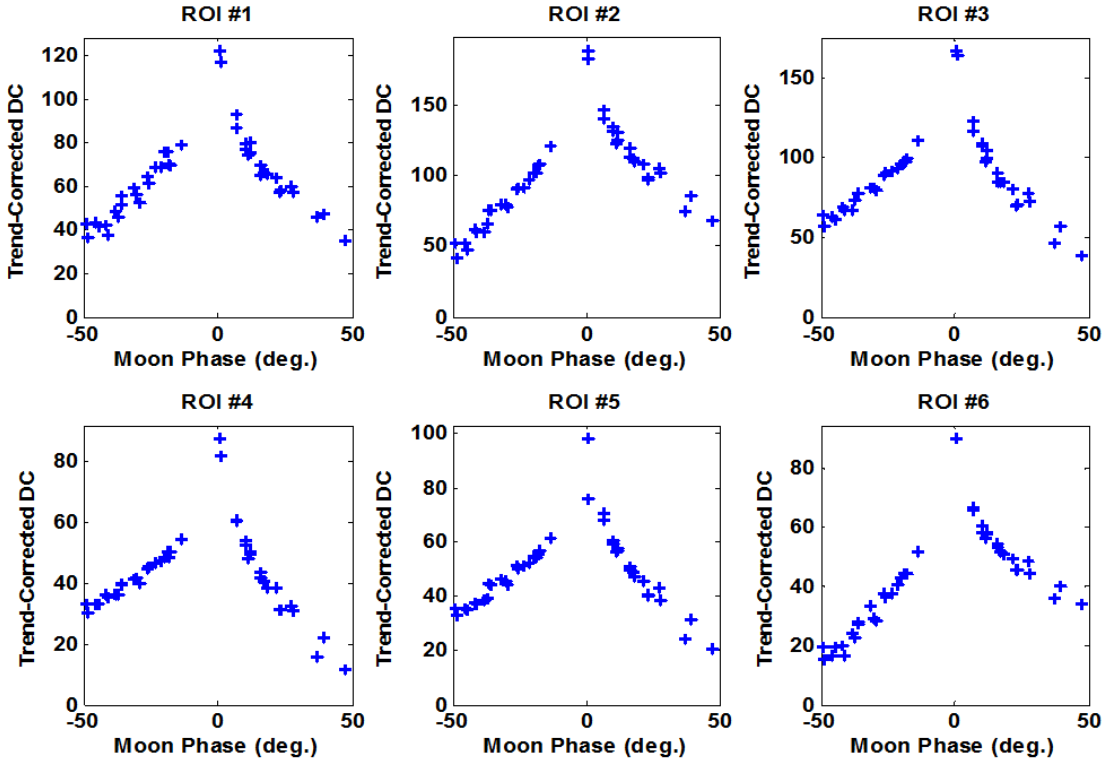

Figure 10: Corresponding lunar measurement (trend-corrected DC) by GOES-12 Imager vs. lunar phase for 6 selected ROIs.

6. SUMMARY

In this paper, we developed algorithm and processing tools to map GOES lunar imagery in visible channel onto selenographic coordinate and showed examples of such mapping for typical cases from GOES-12 observation. A total of 44 lunar observations by GOES-12 Imager with |lunar phase| less than 50 degree have been processed and mapped onto selenographic coordinate. Six ROIs on moon surface were selected and characteristic trend-corrected lunar data over these ROIs were extracted. The characteristic dependence of lunar measurement over ROIs vs. lunar phase angle was investigated. Our study shows strong dependence of trend-corrected lunar data on moon phase and the dependence is asymmetric between waxing and waning lunar phase. This suggests that accurate knowledge of BRDF of lunar surface is important in trending radiometric performance of GOES Imager with lunar radiance. Since lunar images observed by GOES can have different view geometry, different lunar phase, and there are uncertainties in the observation and mapping. Further study will be performed to improve mapping accuracy, implement site selection based on radiometric

property and uniformity, and investigate dependence of lunar radiance on local phase angle of ROIs. Instrument calibration, characterization, and validation are essential to GOES-R satellite mission success and the production of high-quality data products from ABI. Lunar calibration for solar bands is an important part of the GOES-R ABI Cal/Val plan. The mapping tool we developed can enable trending radiometric performance of existing GOES Imager and upcoming GOES-R ABI with lunar radiance, which will be performed in future work.

ACKNOWLEDGMENT

The authors would like to thank for discussion with Changyong Cao and Bin Zhang. The manuscript contents are solely the opinions of the authors and do not constitute a statement of policy, decision, or position on behalf of NOAA or the U.S. government.

REFERENCES

[1] Stone, T. C., H. H. Kieffer, and I. F. Grant. "Potential for calibration of geostationary meteorological imagers using the Moon". Proc. SPIE 5882, 231-239. doi:10.1117/12.620097, 2005.
[2] Stone , T. C., and H. H. Kieffer, "Use of the Moon to support on-orbit sensor calibration for climate change measurements", *Proc. SPIE* 6296, Earth Observing Systems XI, 62960Y, doi:10.1117/12.678605, 2006.
[3] Wu, X., T. Stone, F. Yu, and D. Han, Vicarious calibration of GOES Imager visible channel using the Moon, Proc. SPIE, 6296, doi:10.1117/12.681591, 2006.
[4] Bremer, J., J. Baucom, H. Vu, M. Weinreb, and N. Pinkine, Estimation of long-term throughput degradation of GOES 8 and 9 visible channels by statistical analysis of star measurements, Proc. SPIE, 3439, 145–154, 2006.
[5] Chang, I.-L., C. Dean, D. Han, D. Crosby, M. Weinreb, J. Baucom, P. Baltimore, and X. Wu, Improvements in the star-based monitoring of GOES Imager visible-channel responsivities, Proc. SPIE, 5882, doi:10.1117/12.614601, 2005.
[6] Smith, G., R. Levin, P. Able, and H. Jacobowitz, Calibration of the solar channels of the NOAA-9 AVHRR using high altitude aircraft measurements, J. Atmos. Oceanic Technol., 5, 631–639, 1988.
[7] Cosnefroy, H., M. Leroy, and X. Briottet, Selection and characterization of Saharan and Arabian desert sites for the calibration of optical satellite sensors, Remote Sens. Environ., 58, 101–114, 1996.
[8] Rao, C., and J. Chen, Inter-satellite calibration linkages for the visible and near-infrared channels for the Advanced Very High Resolution Radiometer on the NOAA-7, -9, and -11 spacecraft, Int. J. Remote Sens., 16, 1931–1942, 1995.
[9] Govaerts, Y., M. Clerici, and N. Clerbaux, Operational calibration of the METEOSAT radiometer VIS band, IEEE Trans. Geosci. Remote Sens., 42(9), 1900–1913, 2004.
[10] Wu, X., J. T. Sullivan, and A. K. Heidinger, Operational calibration of the Advanced Very High Resolution Radiometer (AVHRR) visible and near-infrared channels, Can. J. Remote Sens., 36(5), 602–616, 2010.
[11] Yu, F., and X. Wu, Vicarious calibration of GOES Imager visible channels, 2013 EUMETSAT Satellite Conference and 19th AMS Satellite Conference, Vienna, Australia, 16–20 Sept., 2013.
[12] Yu, F., X. Wu, M. Grotenhuis, H. Qian, Inter-calibration of GOES Imager visible channels over the Sonoran desert, Journal of Geophysical Research-Atmosphere, 119, pp. 8639–8659 http://dx.doi.org/10.1002/2013JD020702, 2014.
[13] Yu, F. and X. Wu, An integrated method to improve the GOES Imager visible radiometric calibration accuracy, Remote Sensing of Environment, 164, 103, http://dx.doi.org/10.1016/j.rse.2015.04.003, 2015.
[14] Doelling, D., L. Nguyen, and P. Minnis, On the use of deep convective clouds to calibrate AVHRR data, Proc. SPIE, 5542, 281–289, 2004.
[15] Doelling, D., P. Minnis, and L. Nguyen, Calibration comparisons between SEVIRI, MODIS, and GOES data, MSG RAO Workshop, Salzburg, Austria, 100-11, Sept., 2004.
[16] Wu, X., and F. Sun, Post-launch calibration of GOES Imager visible channel using MODIS data, Proc. SPIE, 5582, doi:10.1117/12.615401, 2005.
[17] Wu, X., H. Qian, F. Yu, and T. Beck , Vicarious calibration of GOES visible channel using GOME-2, in Geoscience and Remote Sensing Symposium (IGARSS), pp. 1033–1035, IEEE, Vancouver, Canada, doi:10.1109/IGARSS.2011.6049310, 2011.

[18] Barnes, R. A., Eplee Jr., R. E., Patt, F. S. and McClain, C. R., "Changes in the Radiometric Sensitivity of SeaWiFS Determined from Lunar and Solar-Based Measurements" . *Appl. Optics,* **(38)21:** 4649-4664, 1999.
[19] Barnes, R., R. Eplee, F. Patt, H. Kieffer, T. Stone, G. Meister, J. Butler, and C. McClain, Comparison of SeaWiFS measurements of the Moon with the U.S. Geological Survey Lunar Model, Appl. Opt., 43, 5838–5854, doi:10.1364/AO.43.005838, 2004.
[20] Kieffer, H. H., and T. C. Stone, "The spectral irradiance of the Moon", *Astron. J.*, 129, 6, 2887, Jun. 2005.
[21] Shao, X., C. Cao, and S. Uprety, Vicarious calibration of S-NPP/VIIRS day-night band, *SPIE Proceedings Vol. 8866, Earth Observing Systems XVIII*, James J. Butler; Xiaoxiong (Jack) Xiong; Xingfa Gu, Editors, 88661S, DOI: 10.1117/12.2023412, 2013.
[22] Shao, X., T. Choi, C. Cao, S. Blonski, W. Wang, Y. Ban, "Trending of Suomi-NPP VIIRS radiometric performance with lunar band ratio", in Earth Observing Missions and Sensors: Development, Implementation, and Characterization III, Xiaoxiong Xiong; Haruhisa Shimoda, Editors, Proceedings of SPIE Vol. 9264 (SPIE, Bellingham, WA), 92640K, 2014.
[23] Shao, X., B. Zhang, C. Cao, "Modeling phase-angle dependence of lunar irradiance using long-term lunar measurements by VIRS on TRMM", in Earth Observing Missions and Sensors: Development, Implementation, and Characterization III, Xiaoxiong Xiong; Haruhisa Shimoda, Editors, Proceedings of SPIE Vol. 9264 (SPIE, Bellingham, WA), 92641E, 2014.
[24] Shao, X. C. Cao, S. Uprety, F. Padula, T. Choi, "Comparing Hyperion Lunar Observation with model calculations in support of GOES-R Advanced Baseline Imager (ABI) calibration", in Earth Observing Systems XIX, James J. Butler; Xiaoxiong (Jack) Xiong; Xingfa Gu, Editors, Proceedings of SPIE Vol. 9218 (SPIE, Bellingham, WA), 92181X, 2014.